Journal of Marine Science and Technology

Volume 24 | Issue 5 Article 9

MECHANICAL BEHAVIORS OF PILED-RAFT FOUNDATION AND DIAPHRAGM WALL IN DEEP EXCAVATION OF TAIPEI METROPOLITAN

Der-Guey Lin
Department of Soil and Water conservation, National Chung-Hsing University, Taichung, Taiwan, R.O.C

Wen-Tsung Liu
Department of Civil Engineering, Kao Yuan University, Kaohsiung, Taiwan, R.O.C

Jui-Ching Chou
Sinotech Engineering Consultants, Taipei, Taiwan, R.O.C, jccchou@mail.sinotech.com.tw

Recommended Citation

Lin, Der-Guey; Liu, Wen-Tsung; and Chou, Jui-Ching (2016) "MECHANICAL BEHAVIORS OF PILED-RAFT FOUNDATION AND DIAPHRAGM WALL IN DEEP EXCAVATION OF TAIPEI METROPOLITAN," *Journal of Marine Science and Technology*: Vol. 24: Iss. 5, Article 9.
DOI: 10.6119/JMST-016-0604-2
Available at: https://jmstt.ntou.edu.tw/journal/vol24/iss5/9

Journal of Marine Science and Technology, Vol. 24, No. 5, pp. 980-991 (2016)
DOI: 10.6119/JMST-016-0604-2

MECHANICAL BEHAVIORS OF PILED-RAFT FOUNDATION AND DIAPHRAGM WALL IN DEEP EXCAVATION OF TAIPEI METROPOLITAN

Der-Guey Lin[1], Wen-Tsung Liu[2], and Jui-Ching Chou[3]

Key words: piled-raft foundation, diaphragm wall, deep excavation, corner effect.

ABSTRACT

The piled-raft foundation has been widely used in recent years to solve the low bearing capacity and the excess settlement problems of the raft foundation on the soft soil. The soft soil is reinforced by the pile and behaviors of the diaphragm wall and the raft are also modified by the pile. However, effects of the pile on the diaphragm wall and the raft have not been fully discussed in the past. In this paper, a finite element program, Plaxis-3D, is used as the numerical simulation tool. First, simulations of pile loading tests are performed to verify the input parameters and models. Then, deep excavation cases with and without the pile group in a typical Taipei Metropolitan soil profile are modeled and discussed to identify effects of the pile. Results show that the pile lowers the lateral displacement of the diaphragm wall, reduces the influence zone of ground settlement around the excavation area and modifies the deformation pattern of the diaphragm wall and ground settlement.

I. INTRODUCTION

The piled-raft foundation is commonly used in Taipei Metropolitan for the high-rise building to provide excellent bearing capacity, transfer large structure loading, and reduce excess settlement of the raft foundation on the soft soil. The piled-raft foundation provides a skillful geotechnical concept which the applied load is transferred by load transferring mechanisms between the pile, the soil and the raft. Because the pile reinforces the soft soil underneath the raft foundation, the behavior of the pile and soft soil combination when subjected to the excavation and loading is different from the behavior of the soft soil only. This change obviously affects the behavior of the diaphragm wall and the raft when they are subjected to the excavation and the vertical structure loading. Many researchers used different numerical tools to study the behavior of the piled-raft foundation (Chen, 2002; Comodromos et al., 2009; Oh et al., 2009; Lee et al., 2010; Poulos et al., 2011; Bourgeois et al., 2012; Karim et al., 2013; Nguyen et al., 2014). However, the effect of the pile on the diaphragm wall and the raft has not been fully investigated in the past.

In Taiwan, despite the adverse geological conditions, the high-rise building construction project using the piled-raft foundation has become popular. The safety and economy of the piled-raft foundation project is then getting more attention. Accordingly, accurately determining the behavior of such complex foundation is critical and the designers must consider the interaction between the pile, the soil and the raft.

This paper attempts to identify effects of the pile on the diaphragm wall and the raft in a typical soil profile of Taipei Metropolitan. In order to solve the complex problem of the piled-raft foundation, many researchers have applied various methods to analyze piled-raft foundations. From available literatures (Oh et al., 2009; Lee et al., 2010; Poulos et al., 2011; Karim et al., 2013; Nguyen et al., 2014), the three-dimensional (3-D) finite element program, Plaxis-3D, can well capture interaction behaviors of the pile, the soil and the raft and deliver reasonable and reliable simulation results for mechanical behaviors of the piled-raft foundation. Therefore, Plaxis-3D was used in this study to model the piled-raft foundation. In order to perform a 3-D numerical simulation of the foundation rationally, the calibration of 3-D numerical model and input material model parameters become crucial and necessary. Pile loading test results in the jobsite of *TIFC* (*Taipei International Financial Corporation* or *Taipei 101*) are used for the calibration of the numerical model and relevant inputs. Eventually, the piled-raft and the unpiled-raft foundations of several cases situated in a typical soil profile of Taipei Metropolitan are analyzed and discussed.

Paper submitted 10/12/15; revised 05/09/16; accepted 06/04/16. Author for correspondence: Jui-Ching Chou (e-mail: jccchou@mail.sinotech.com.tw).
[1] Department of Soil and Water conservation, National Chung-Hsing University, Taichung, Taiwan, R.O.C.
[2] Department of Civil Engineering, Kao Yuan University, Kaohsiung, Taiwan, R.O.C.
[3] Sinotech Engineering Consultants, Taipei, Taiwan, R.O.C.

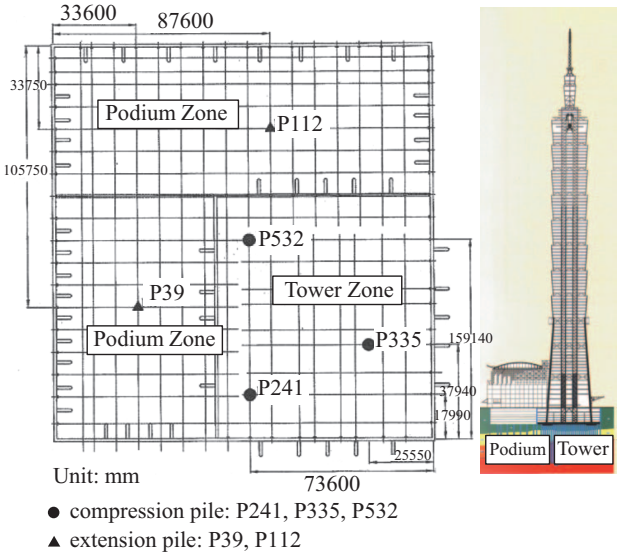

Fig. 1. Plan view of excavation zone and location of testing piles.

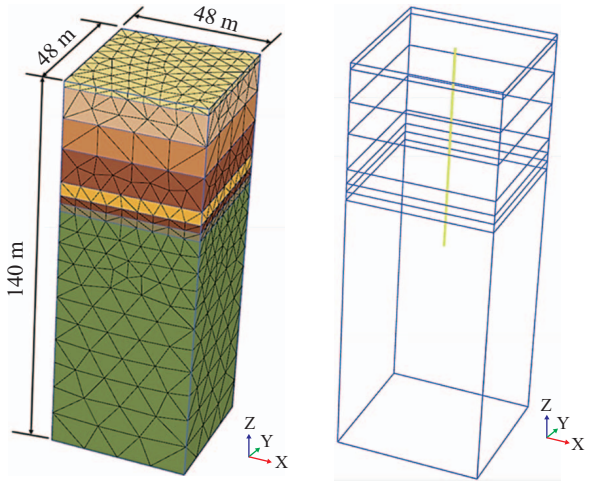

(a) FEM mesh and soil strata (b) Testing pile and soil strata

Fig. 2. 3-D numerical model of pile loading test.

Table 1. Input material model parameters of soil layers and testing pile.

Depth Soil layer (*SPT*)	c' (kPa)	ϕ' (°)	ν'	E' (MPa)	$\frac{\gamma_d}{\gamma_{sat}}$ (kN/m^3)	ψ (°)	R_{inter}
0~2.2 m SF (N = 4~12)	10.0	35	0.30	7.5	17.15 / 18.13	5	0.85
2.2~13.4 m CL1a (N = 2~5)	22.5	31	0.30	14.1	18.33 / 18.53	0	0.90
13.4~24.5 m CL1b (N = 3~6)	24.0	33	0.30	17.4	18.72 / 19.32	0	0.90
24.5~37.0 m CL1c (N = 5~15)	23.0	32	0.30	19.6	18.48 / 18.74	0	0.90
37.0~42.0 m SM (N = 12~34)	20.0	37	0.30	75.0	19.35 / 20.03	1	0.90
42.0~45.0 m CL2 (N = 8~18)	25.0	35	0.30	15.7	18.62 / 18.91	5	0.90
45.0~48.0 m GC-GM (N > 100)	30.0	39	0.30	270	20.75 / 22.08	2	0.95
48 m ~ SS (N > 100)	79.4	45	0.25	680	20.57 / 20.64	0	0.95
Testing Pile	L_p (m)	D_p (m)	ν_p	E_p (MPa)	γ_p (kN/m^3)	-	
P39	70.7	2.0	0.19	33000	23.5	-	
P241	72.8	1.5	0.19	33000	23.5	-	

*R_{inter}: The strength reduction factor for the interface between the embedded pile and the soil. $c_{interface} = R_{inter} \times c_{soil}$, $\tan\phi_{interface} = R_{inter} \times \tan\phi_{soil}$.

SF = Surface Fill; CL = Low Plasticity Clay; SM = Silty Sand; GC-GM = Clayey Gravel to Silty Gravel; SS = Sand Stone

II. PILE LOADING TEST SIMULATION

As shown in Fig. 1, *Taipei 101* Construction Project (or *Taipei 101*) possesses a deep excavation at Tower Zone and Podium Zone with total excavation area of 152.20 m × 159.14 m × 21.7 m. A total of 508 bored piles were installed beneath the raft foundation of the basement. In *Taipei 101*, five pile loading tests (three extension piles, P241, P335 and P532, and two compression piles, P39, P112) were carried out at the initial design stage. The testing piles were instrumented with strain gauges and rebar transducers to estimate the load distribution and deformation. In this study, comparisons between field measurements and numerical simulations of pile loading test for compression pile P241 and extension pile P39 are made to validate the suitability and reliability of numerical procedures and input parameters for Plaxis-3D program used to simulate the soil-pile interaction behaviors when subjected to a vertical loading. Interaction behaviors include load-settlement curves of the pile head, pile shaft and pile tip and load-transfer curves of the pile shaft.

The geometry and soil profile used for the 3-D numerical model of the static pile loading test are shown in Fig. 2. The geometry dimensions of the numerical model are 48 m × 48 m × 140 m (= length × width × height), in which, the length and the width of 48 m are equivalent to 24 × D_p (D_p = pile diameter = 2 m) and the height of 140 m equals to 2.0 × L_p (L_p = pile length = 70 m). These dimensions were inspected and considered to be adequate to eliminate the influence of boundary effects on the performance of loading pile.

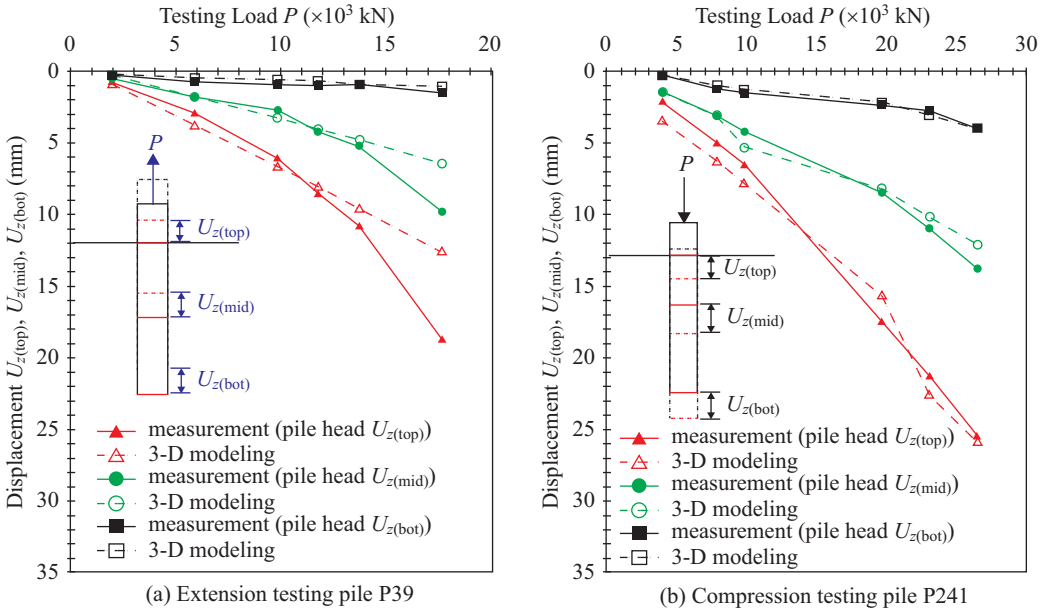

Fig. 3. Load-ground settlement curves.

The pile and soil are modeled with finite elements, which allow for rigorous treatment of soil-pile interaction. The soil behavior is simulated by Mohr-Coulomb model and the testing pile is modeled using the embedded pile element. The embedded element of Plaxis-3D is defined as a massive circular pile and considered as a linear-elastic material. Lee et al., (2010) showed the embedded pile to be a convincing tool to simulate the piled raft systems.

The soil strata of *Taipei 101* jobsite and the associated engineering properties of soil materials are based on high quality field test results and laboratory test results (using undisturbed soil samples) from the relevant project reports (Lin and Woo, 2000, 2005). The typical subsoil in *Taipei 101* jobsite was generalized into eight layers. The Young's modulus of soil layer were determined through back analysis of pile loading testing data of *Taipei 101* construction project by fitting the load-settlement curves and load-transfer curves of the numerical simulation with the measurement. Input soil and pile material model parameters are listed in Table 1. Soil material includes: SPT-N value (N), cohesion (c'), friction angle (ϕ'), Poisson's ratio (ν'), Young's modulus (E'), dry unit weight (γ_d), saturated unit weight (γ_{sat}) and dilation angle (ψ). Pile material includes: length (L_p), diameter (D_p), Poisson's ratio (ν_p), Young's modulus (E_p) and unit weight (γ_p). The embedded pile element is assumed to behave as a linear-elastic material with no failure limit.

The simulation of the static pile loading test followed the Standard Loading Procedure of ASTM D3689-83 for the extension pile P39 and the Standard Loading Procedure of ASTM D1143-81 for the compression pile P241. Comparisons were made between the measured and the simulated load-settlement curves (P~u_z curves) and load-transfer curves (Q~z curves).

Fig. 3 shows comparisons between the measured and the simulated P~u_z curves at the pile head, pile shaft and pile tip for the extension pile P39 and the compression pile P241. The simulations of P39 are in good agreement with measurements except at a higher loading level (P > 14 MN) where the corresponding settlement is under predicted. This deviation may be caused by the limitation of Mohr-Coulomb soil model which is unable to properly simulate the large extension failure of soil/pile interface nearby the pile head. Nevertheless, the simulation of pile P241 is in excellent agreement with measurements.

Fig. 4 displays the comparisons between the measured and the simulated Q~z curves for the extension pile P39 and the compression pile P241. The predicted Q~z curves for P39 and P112 are fitting very well with measurements.

Conclusively, the embedded pile element can capture the deformation and load-transfer behaviors of the pile fairly well and the above numerical procedures and input model parameters are justified and valid to use in the sequential analyses.

III. PILED-RAFT AND UNPILED-RAFT FOUNDATION

In this section, behaviors of the piled-raft foundation and the unpiled-raft foundation subjected to excavation and structure loading are modeled and discussed. The cross sectional profile of the numerical model used for the simulation of the piled-raft and the unpiled-raft foundation is shown in Fig. 5. L_P is the pile length and L_R is the length of raft foundation (L_R = 48 m, 72 m and 120 m).

As shown in Fig. 5, dimensions of the numerical model are 220 m × 220 m × 220 m. The left and right boundaries of the model are extended at least 4 times of the excavation depth (12 m) from the left and right edges of the raft foundation. The bottom boundary is extended about 4 times of the pile length

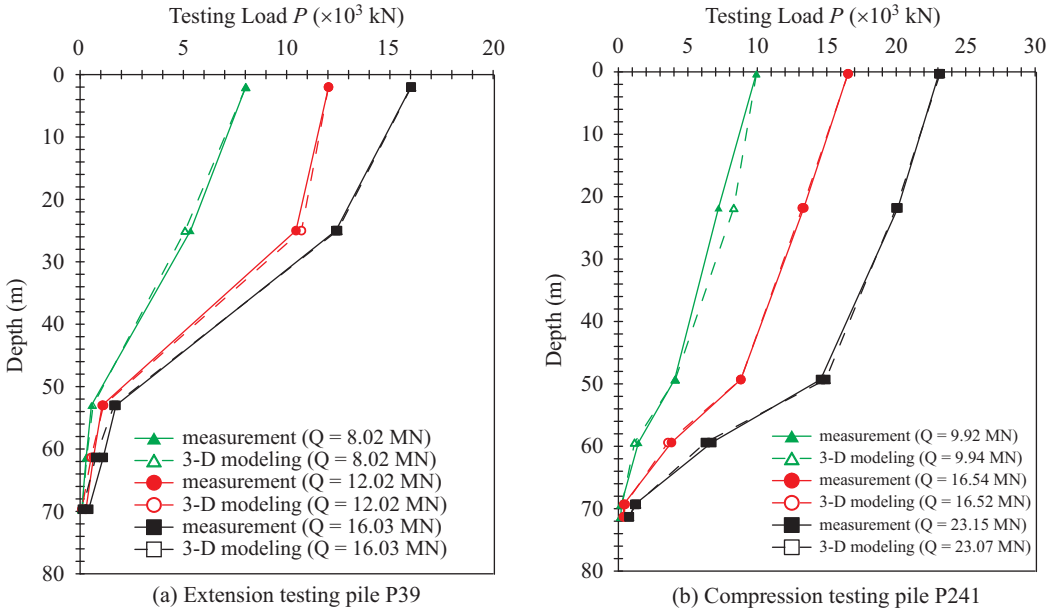

Fig. 4. Comparison between measurement and modeling of loadtransfercurves.

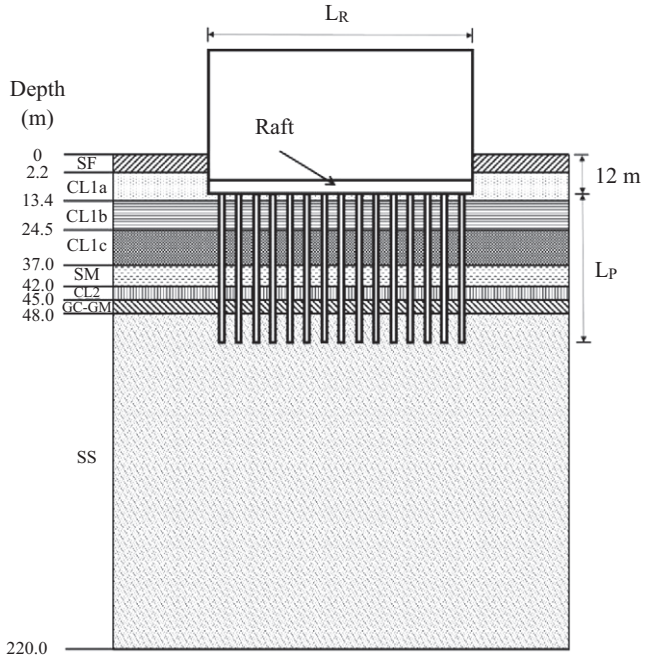

Fig. 5. Plan view of the piled-raft foundation (L_P = 35m)and the un-piled-raft foundation (L_P = 0m).

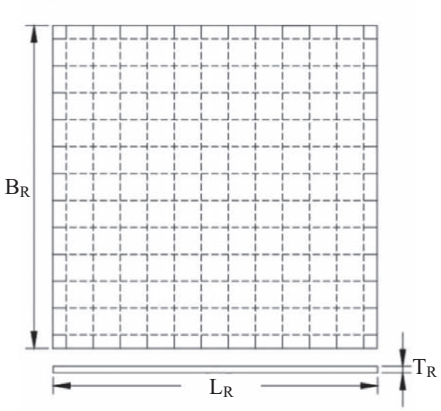

Fig. 6. Dimensions of raft foundation.

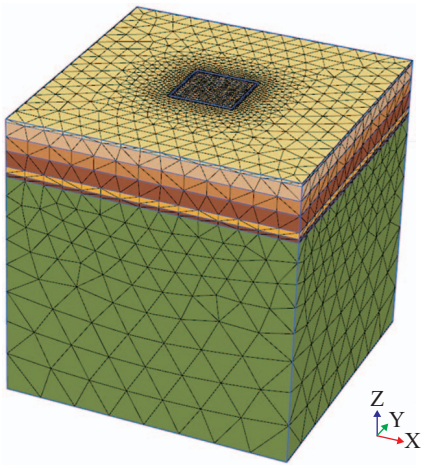

Fig. 7. Finite element mesh for deep excavation with piled-raft foundation.

(= L_P = 35 m) from the pile tip. These dimensions are considered adequate to eliminate the influence of boundary effects on interaction behaviors of the pile and the diaphragm wall. Fig. 6 shows dimensions of the raft foundation. The length, width and thickness of the raft are denoted as L_R, B_R and T_R respectively. For the piled-raft foundation, the spacing of piles is 4 m (= S_p) and the distance from outskirt pile to raft edge is 2 m. The finite element mesh of the numerical model is shown in Fig. 7.

Table 2. Input model parameters of supporting structures and pile.

Supporting Structure	Diaphragm Wall	Floor Slab	Raft	H-Beam	Pile
Thickness t (m)	1.2	0.38	1.0	---	---
Cross section area A (m^2)	---	---	---	0.0219	3.142
Diameter D (m)	---	---	---	---	2.0
Unit Weight γ (kN/m^3)	23.5	23.5	23.52	76.94	24.09
Young's Modulus E (MPa)	25100	25100	33000	400	36000
Poissonratio ν	0.15	0.15	0.15	---	---
Moment of inertia I ($\times 10^{-3}$ m^4)	---	---	---	$I_x = 6.66$ $I_y = 2.24$	$I_x = 785$ $I_y = 785$

In simulations of the piled-raft and the unpiled-raft foundation, input parameters of soil layers are listed in Table 1. Excavation supporting structures of the model include diaphragm wall, floor slab, H-beam (columns of floor), and raft foundation. Diaphragm wall, floor slab and raft foundation are modeled using the plate element while H-Beam is modeled by the beam element. Behaviors of these supporting structures are assumed to be elastic and isotropic. Material properties of supporting structures and the pile structure are listed in Table 2.

In simulations of piled-raft and the unpiled-raft foundations, the effect of *R*aft *S*ize *F*actor ($RSF = B_R/L_R$ = width/length) is also discussed and three cases of $RSF$are: RSF = 48 m/48 m = 1.00, 48 m/72 m = 0.67 and 48 m/120 m = 0.40. The construction sequences of deep excavation for each case are as followed : (1) Phase 1 - generate initial stress, (2) Phase 2 - install diaphragm wall (length = 36 m), H-beam (floor columns) and piles (diameter = 2 m) for the piled-raft foundation, (3) Phase 3 - excavate to a depth of 12 m and install the raft foundation, and (4) Phase 4 - apply the structure loading to the raft foundation. The structure loading is simulated by the typical loading intensity (3-story, 6-story, 9-story, 12-story of the superstructure) of a residential building suggested by Liang et al. (2003). Loading intensities of 3-story, 6-story, 9-story and, 12-story of the superstructure are 98.56 kN/m^2, 147.8 kN/m^2, 197.1 kN/m^2, and 246.4 kN/m^2 respectively. Following sections discuss interaction behaviors of the piled-raft and the unpiled-raft foundation simulated in Phase 3 and Phase 4.

1. Phase 3 - Excavation

The lateral diaphragm wall displacement (δ_h), plain strain ratio (PSR) and ground settlement (δ_v) induced from the deep excavation (at the end of Phase 3) are discussed in this section.

Fig. 8 shows the lateral displacement contour of the diaphragm wall ($RSF = B_R/L_R$ = 1.0, $L_R = B_R$ = 48 m) located at the raft edge with length of (L_R) at the end of Phase 3. Because the lateral wall displacement is symmetrical to x-axis and y-axis and the lateral wall displacement at the raft length (L_R) side is equal or greater than that at the raft width (B_R) side, as a consequence, only lateral wall displacements of representative sections along the diaphragm wall at the raft length (L_R) side (x = 0~0.5 L_R = 0~24 m, y = 24 m; see Fig. 9) are discussed.

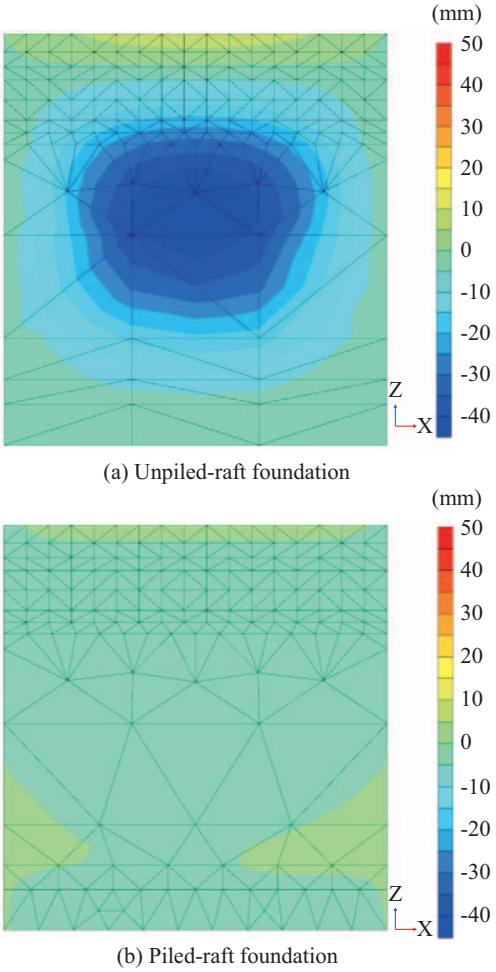

Fig. 8. Lateral wall displacement contour of diaphragm wall.

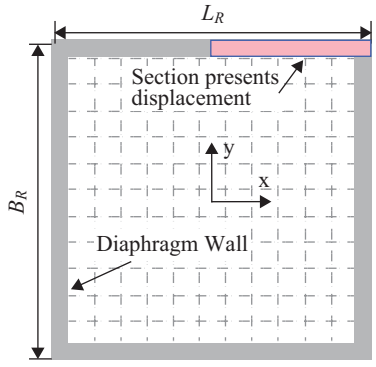

Fig. 9. Representative sectionsof diaphragm wall.

Table 3. Maximum lateral wall displacement for different *RSF*.

RSF (= B_R/L_R)	1.00	0.67	0.40
Unpiled-Raft			
$(\delta_{h\text{-}max})_{3D}$*(mm)	44.54	59.68	67.60
Piled-Raft			
$(\delta_{h\text{-}max})_{3D}$*(mm)	12.83	14.64	15.76
* 3-D maximum lateral wall displacement. Diaphragm wall length = 36 m, Excavation depth = 12 m			

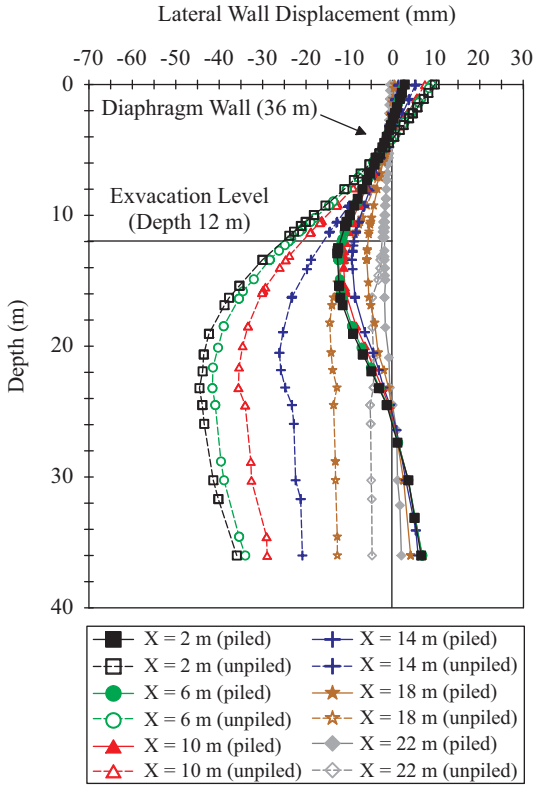

Fig. 10. Lateral wall displacementat representative sections for the case of *RSF* = 1.0.

Figs. 10-12 show results of lateral wall displacements at representative sections for three *RSF*s cases (*RSF* = 1.00, 0.67 and 0.40). Maximum lateral wall displacements, $(\delta_{h\text{-}max})_{3D}$, are summarized in Table 3.

Comparing results of the piled-raft and the unpiled-raft foundations in Figs. 10-12, the pile group beneath the raft foundation not only lowers the lateral wall displacement but also changes the displacement pattern. The $(\delta_{h\text{-}max})_{3D}$ values of piled-raft foundations approximate 25% of those of unpiled-raft foundations in deep excavation. The location of the maximum lateral displacement moves from a depth near the middle of the diaphragm wall (depth of 20~24 m) of unpiled-raft cases to a depth just below the excavation level (depth of 14 m) of piled-raft cases. The possible cause could be that the pile group reinforces the soil underneath the raft foundation and prevents

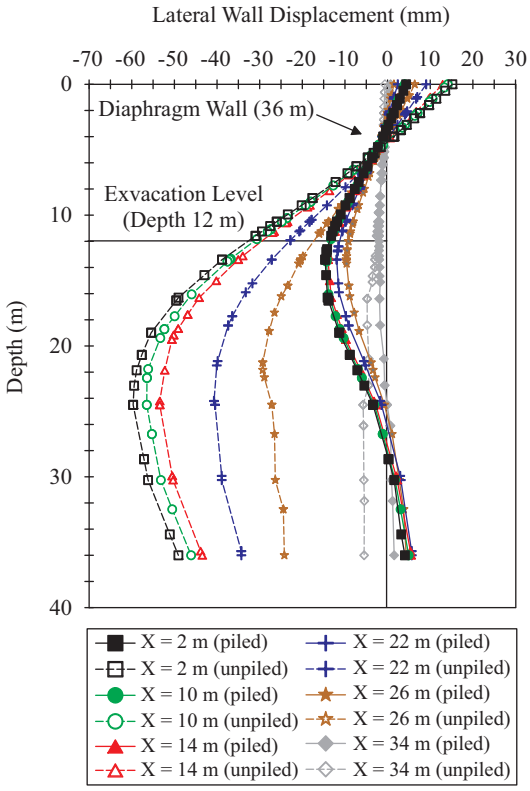

Fig. 11. Lateral wall displacement at representative sections for the case of *RSF* = 0.67.

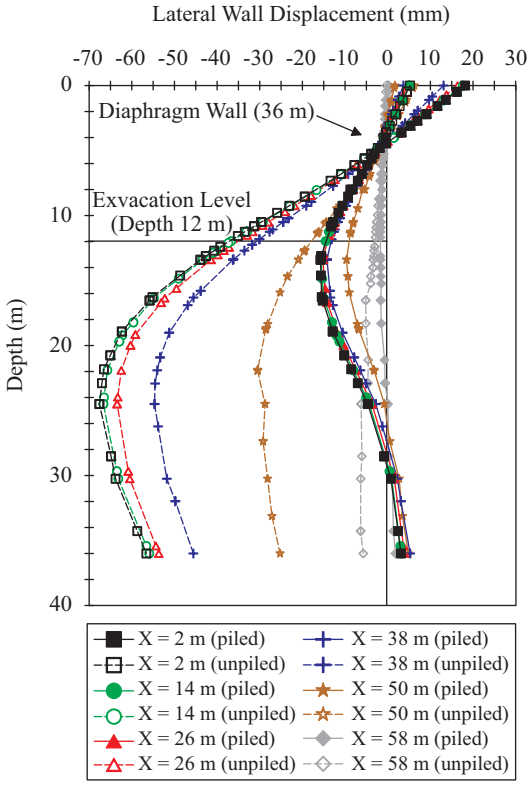

Fig. 12. Lateral wall displacementat representative sections for the case of *RSF* = 0.4.

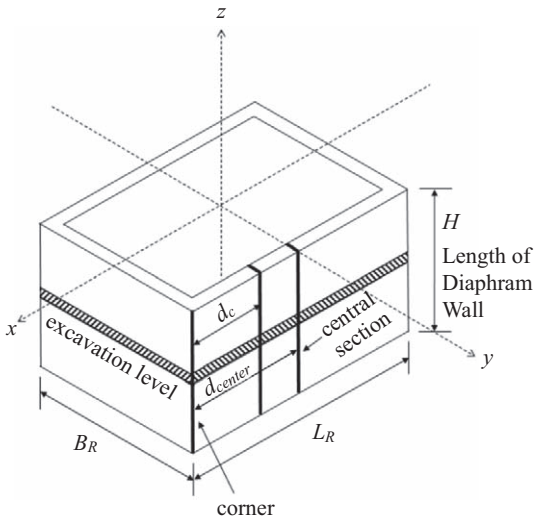

Fig. 13. Illustration for selected sections along diaphragm wall.

the soil mass behind the diaphragm wall from squeezing into the excavation area. This effectively lowers the lateral wall displacement and also imposes an upward shifting of the location of maximum lateral wall displacement. Therefore, neglecting the pile foundation in numerical model may reduce the retaining capacity of the diaphragm wall and consequently leads to a larger lateral wall displacement.

In addition, the wall displacement pattern of unpiled raft cases in Figs. 10-12 show that the tip of the diaphragm wall still experiences about 80% of the maximum wall displacement. The possible cause might be that the tip of the diaphragm wall still rests on the soft clay layer (CL1c) rather than on the sand stone layer (SS) and the soft clay layer has no enough stiffness and strength to constrain the movement of the diaphragm wall.

In engineering practice, the lateral wall displacement of a deep excavation is usually estimated by using the plane strain analysis because the analysis constantly gives a conservative result. The plane strain analysis assumes that the lateral wall displacement is not affected by the restrain effect of the corner and the corner effect does not occur in plane strain analysis. However, comparing lateral wall displacements of different *RSF* cases, the corner effect (or three-dimensional effect) of lateral wall displacement becomes significant when the *RSF* value decreases. Fig. 13 illustrates the selected section of diaphragm wall for plain strain ratio (*PSR*) analyses. In which, d_c represents the distance of selected sections away from the wall corner and d_{center} is the distance of central section away from the wall corner. Because of the symmetry of the lateral wall displacement, only the sections along the diaphragm wall on the raft length (L_R) side (y = 0.5, B_R = 24 m, B_R = 48 m; x = 0~0.5 L_R, L_R = 48 m)are presented.

The *PSR* value for a selected section situated at a distance of (d_c) away from the corner can be calculated as follows:

$$PSR = \left(\delta_{h-\max}\right)_{3D} / \left(\delta_{h-\max}\right)_{2D} \quad (1)$$

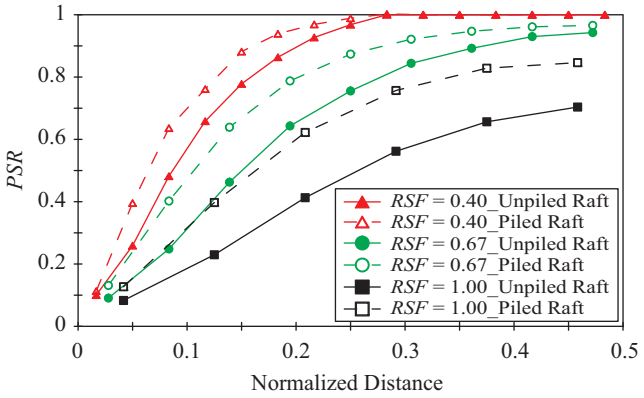

Fig. 14. Plane strain ratio variation for different cases of *RSF*.

where $(\delta_{h\text{-}max})_{3D}$ is the maximum lateral wall displacement of selected section obtained from 3-D analysis and $(\delta_{h\text{-}max})_{2D}$ is the maximum lateral wall displacement of selected section obtained from 2-D plane strain analysis. In this study, the displacement at the central section of *RSF* = 0.4 case is used as $(\delta_{h\text{-}max})_{2D}$. A lower *PSR* value represents a higher corner effect exists.

Fig. 14 shows the variation of the plane strain ratio (*PSR*) of the selected section with the normalized distance (d_c/L_R). The figure shows that the *PSR* of unpiled-raft cases is constantly smaller than that of piled-raft cases ($PSR^{unpiled} \leq PSR^{piled}$). As listed in Table 3, maximum lateral wall displacements, $(\delta_{h\text{-}max})_{3D}$, of piled-raft cases approximate 25% of those of unpiled-raft cases (or $(\delta_{h\text{-}max})_{3D}^{piled} \approx 0.25 \times (\delta_{h\text{-}max})_{3D}^{unpiled}$). Incorporating Fig. 14 with the *PSR* in Eq. (1), it can be deduced that the maximum lateral wall displacement of plane strain condition, $(\delta_{h\text{-}max})_{2D}$, of piled-raft cases is smaller than 25% of that of unpiled-raft cases (or $(\delta_{h\text{-}max})_{2D}^{piled} < 0.25 \times (\delta_{h\text{-}max})_{2D}^{unpiled}$) or the maximum lateral displacement of unpiled-raft cases is larger than 4 times of that of the piled-raft cases (or $(\delta_{h\text{-}max})_{2D}^{unpiled} > 4.0 \times (\delta_{h\text{-}max})_{2D}^{piled}$).

Fig. 15 displays the ground settlement contour after the deep excavation for the piled-raft foundation with *RSF* = 1.0. Because the distribution of ground settlement is symmetrical both along the raft width (B_R) and the raft length (L_R), only numerical results of ground settlement (δ_v) along the half of the raft length (L_R) are presented in this paper.

Figs. 16-18 show the ground settlement, (δ_v), after the deep excavation. The left half and right half of figures illustrate ground settlements for the piled-raft and the unpiled-raft cases respectively. The ground settlement troughs from the diaphragm wall to a distance of 26 m away from the wall (about 2 times of excavation depth) are plotted. Results of piled-raft cases show that the magnitude and pattern of ground settlement are similar for different *RSF*s. This is resulted from the array of group piles reinforces the soil underneath the excavation level which alternately suppresses the ground settlement. For unpiled-raft cases, the magnitude of ground settlement decreases as the *RSF* increases and which is similar to the behavior of lateral wall displacement.

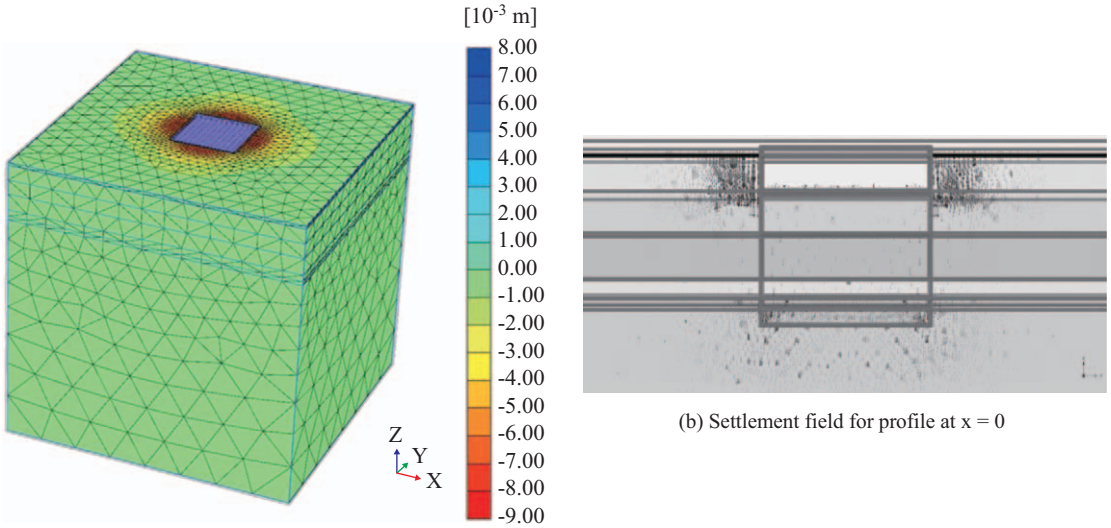

(a) Settlement contour of 3-D model

(b) Settlement field for profile at x = 0

Fig. 15. Ground settlement after deep excavation for the piled-raft foundation with *RSF* = 1.0.

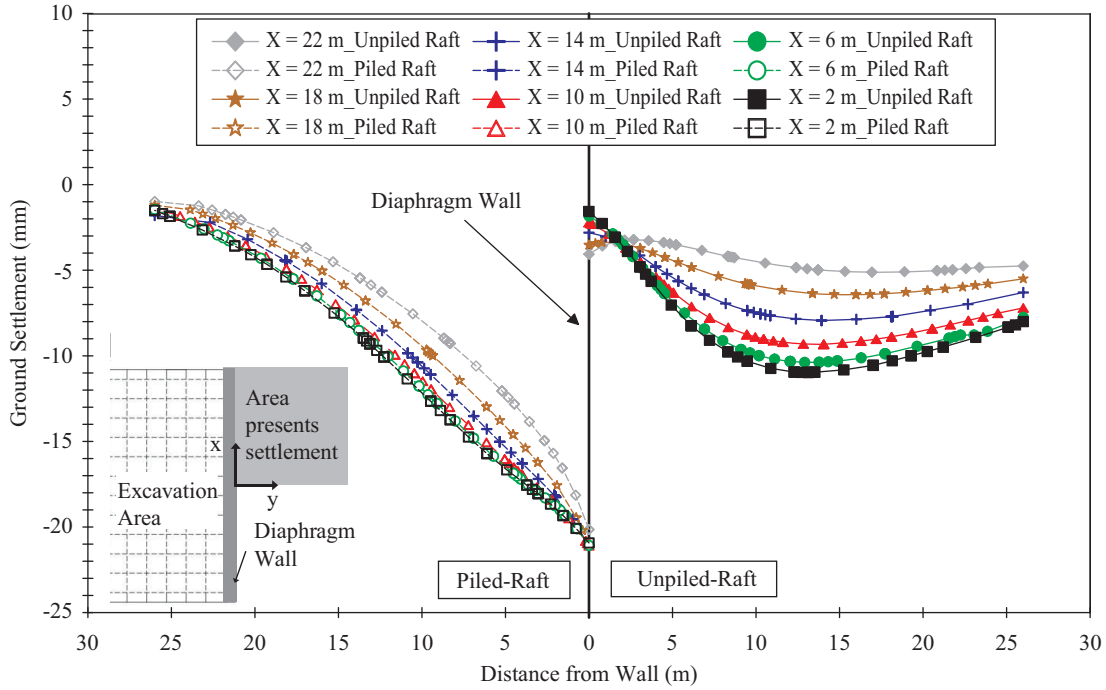

Fig. 16. Ground settlement contour of deep excavation for the piled-raft (left half of figure) and unpiled-raft (right half of figure) foundation with *RSF* = 1.0.

Other than the magnitude of ground settlement, the settlement pattern of the piled-raft case is different from that of the unpiled- raft case. Because the pile group underneath the excavation level promotes the overall stiffness of the soil mass which alternately increases the retaining effect at the bottom of diaphragm wall. Eventually, the diaphragm wall reveals a cantilever type of lateral displacement and accompanied with a spandrel pattern of ground settlement (Hsieh and Ou, 1998). The maximum ground settlement $(\delta_{v\text{-}max})_{3D}$ occurs next to the wall and the ground settlement decreases to $0.1 \times (\delta_{v\text{-}max})_{3D}$ at a distance of 26 m away from the wall.

On the contrary, for the unpiled-raft case, without reinforcement of pile group underneath the excavation level, the diaphragm wall exhibits a bulge type of lateral displacement and accompanied with a concave pattern of ground settlement (Hsieh and Ou, 1998). The $(\delta_{v\text{-}max})_{3D}$ value occurs at a dis-

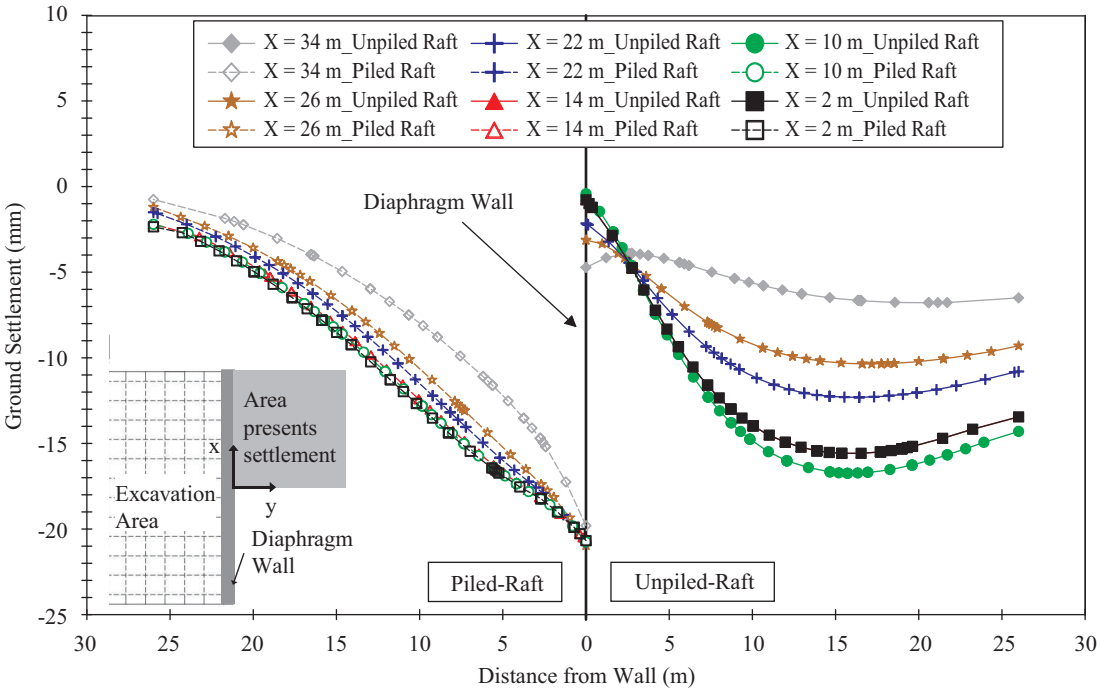

Fig. 17. Ground settlement contour of deep excavation for the unpiled-raft (right half of figure) and piled-raft (left half of figure) foundation with *RSF* = 0.67.

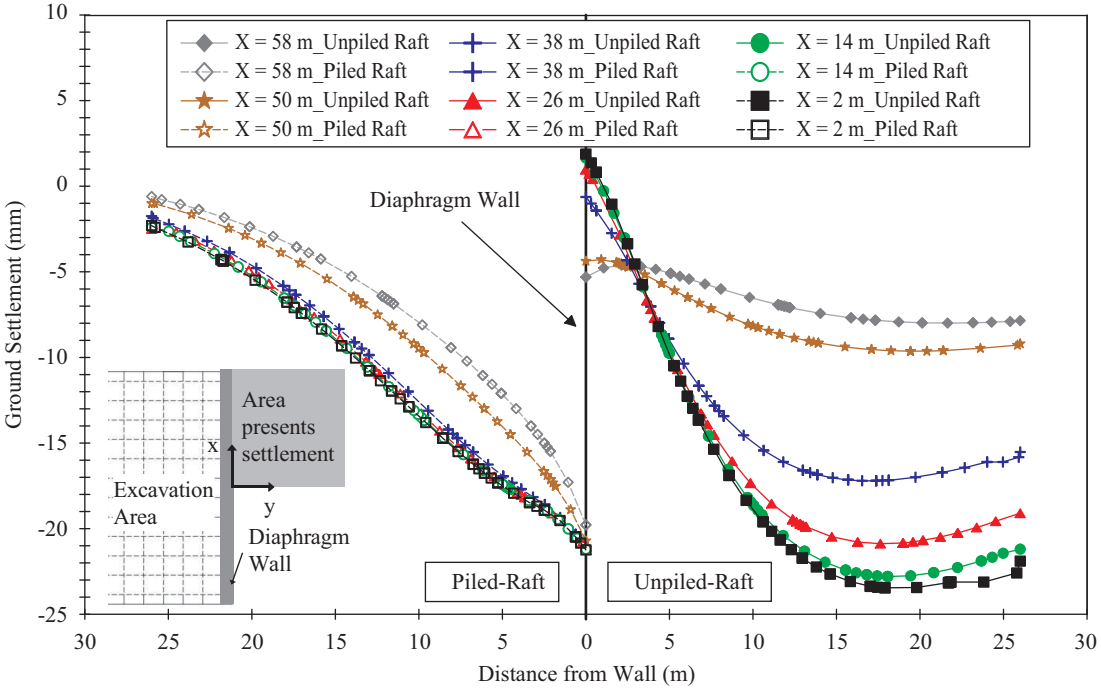

Fig. 18. Ground settlement contour of deep excavation for the piled-raft (left half of figure) and unpiled-raft (right half of figure) foundation with *RSF* = 0.4.

tance of 15~17 m (≈ one excavation depth) away from the wall and the ground settlement decreases to 0.8 × $(\delta_{v\text{-}max})_{3D}$ at a distance of 26 m away from the wall.

Fig. 19(a) shows the measured ground settlement of *Taipei 101* with the piled-raft foundation (Chou, 2002) at different locations and it can be considered as the settlement pattern of the piled-raft case. On the contrary, Fig. 19(b) presents the simulated ground settlement with the unpiled-raft using FLAC3D

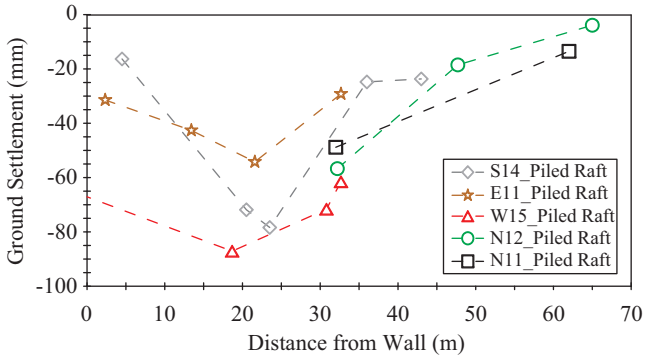

(a) Measured ground settlement (with piled-raft foundation)

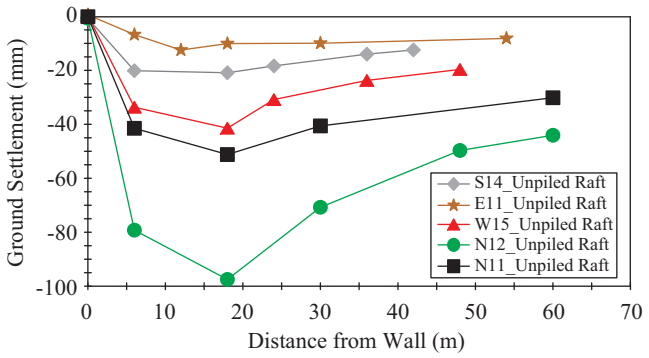

(b) Simulated ground settlement (with unpiled-raft foundation)

Fig. 19. Comparison of ground settlement between measurement and FLAC3D simulation.

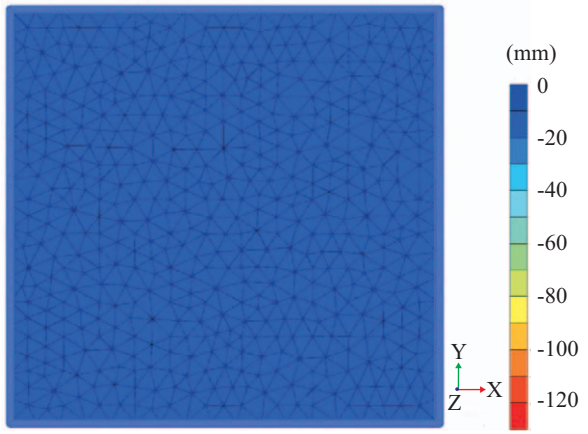

(a) The piled-raft foundation

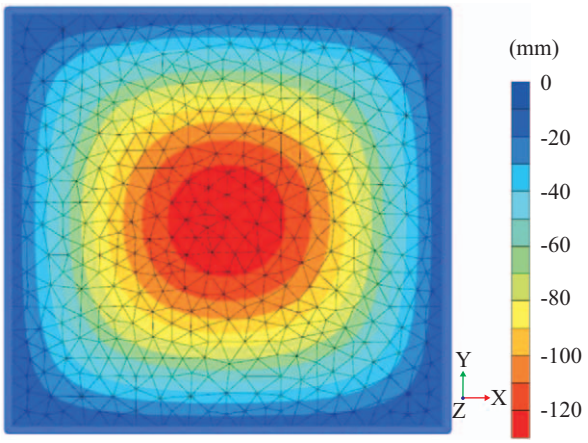

(b) The unpiled-raft foundation

Fig. 20. Raft settlement contour subjected to vertical loading.

(Chou, 2002) and it can be seen as the settlement pattern of the unpiled-raft case. Comparing the ground settlement patterns of Figs. 16-18 with Fig. 19, the ground settlement patterns of piled-raft and unpiled-raft foundations in this study are similar to those presented by Chou (2002).

The influence zone of ground settlement (ground surface experiences a settlement larger than 0.1 × $\delta_{v\text{-}max}$) is wider in unpiled-raft cases due to a larger scale of soil mass behind the wall is squeezed into the excavation area. On the other hand, in piled-raft cases, the influence zone of ground settlement is much less because of the soil mass underneath the excavation level is largely reinforced by pile group.

2. Phase 4 – Structure Loading

This section discusses the settlement and bending moment of the piled-raft and the unpiled-raft with RSF = 1.0 under a vertical loading equivalent to a 12-F (12 Floors) superstructure.

Fig. 20 displays settlement contours of the piled-raft and the unpiled-raft foundations subjected to the structure loading. The settlement of the piled-raft foundation is much smaller than that of the unpiled-raft foundation. Because of the bi-lateral symmetry of the raft, only one quarter (1/4) of the raft settlement profiles at selected sections (x = 2, 9, 16 and 23) are shown in Fig. 21. A normalized settlement is presented for a better demonstration of the settlement pattern. The normalized settlement (S/S_{max}) is defined as the ratio of raft settlement (S) to maximum raft settlement (S_{max}) for the unpiled-raft case ($S_{max\text{-}unpiled}$ = 139.28 mm)and the piled-raft case ($S_{max\text{-}piled}$ = 17.29 mm) respectively. As shown in Fig. 21, the raft settlement is gradually increasing from the raft edge to the raft center. The maximum raft settlement occurs at the central area of the raft within a range of $x = \pm 0.2\ L_R$ and $y = \pm 0.2\ B_R$. Comparing the magnitude and settlement pattern between the piled-raft and the unpiled-raft cases, the settlement and the angular distortion of the piled-raft is greatly reduced by the pile group. For the case of RSF = 1.0, the pile group enables to reduce the maximum raft settlement from 139.28 mm to 17.29 mm (a reduction of 88%) and the maximum angular distortion from 1/146 to 1/1850. Similar observations were found by previous researches (Long, 2010; Karim et al., 2013; and Nguyen et al., 2013).

Fig. 22 presents the variation of bending moments (along x = 2 m and y = –24 m~24 m) of rafts subjected to a vertical loading equivalent to a 12-Floor superstructure. In general, the raft bending moment pattern is similar to the raft settlement pattern. For the unpiled-raft, the raft appears a concave settlement pattern at the central area (see Fig. 20(b)) which

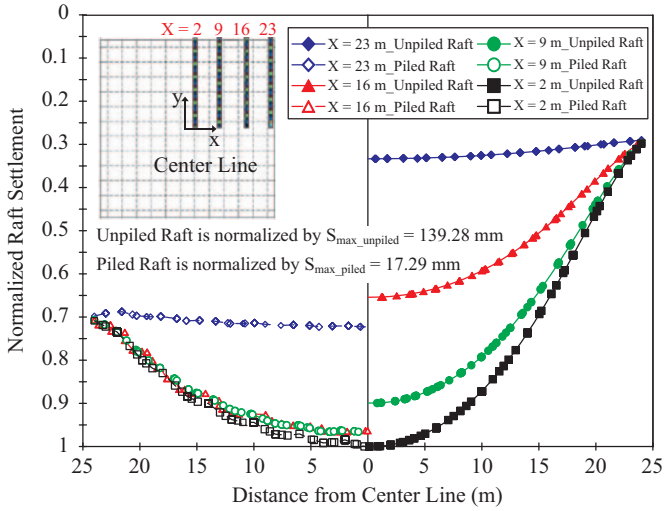

Fig. 21. Raft settlement profile under 12-F vertical uniform loading.

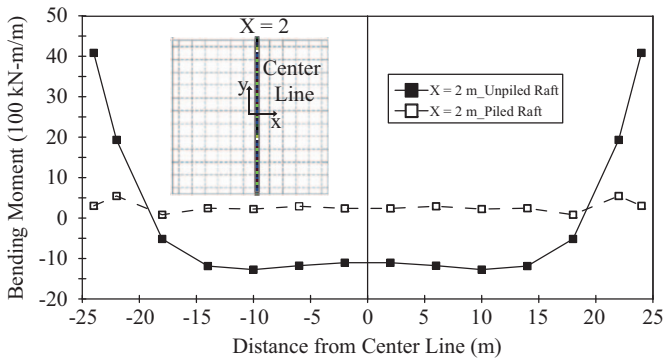

Fig. 22. Raft bending momentunder 12-F vertical uniform loading.

alternately accompanied by a larger bending moment (see Fig. 22). On the contrary, for the piled-raft, the raft shows a uniform settlement pattern (see Fig. 20(a)) due to an equally spacing pile group installed beneath the raft which consequently associated with a smaller bending moment pattern. Definitely, the differential settlement of the unpiled-raft, which is much larger than that of the piled-raft, is the main cause to develop a relatively high bending moment. The pile group enables to reduce the maximum bending moment of the raft from 40.8×10^2 kN-m to 5.5×10^2 kN-m (a reduction of 87%). In conclusions, the pile group is a very effective facility to reduce the settlement, angular distortion and bending moment of raft.

IV. CONCLUSIONS

The piled-raft foundation is used to solve the low bearing capacity and the excess settlement problems of the raft foundation on the soft soil. Many researchers used different numerical tools to study interaction behaviors of the piled-raft foundation. However, effects of the pile group on interaction behaviors of the diaphragm wall and the raft in the deep excavation are not fully discussed in the past. This paper investigates the effect of the pile on the diaphragm wall and the raft in a typical soil profile of Taipei Metropolitan using the 3-D finite element method.

Numerical simulations of two pile loading tests in the jobsite of *Taipei 101* are used to calibrate numerical procedures and relevant material model input parameters. Subsequently, the piled-raft and unpiled-raft foundation cases are analyzed and discussed. In the simulation of pile loading tests, incorporating with the Mohr-Coulomb soil model and the embedded pile element can capture the load-settlement curve and load-transfer curve of the extension pile P39 and the compression pile P241 in excellent coincidence.

In the deep excavation phase, the pile group beneath raft foundation not only lowers the lateral wall displacement but also changes the displacement patterns of diaphragm wall. Due to the fact that the pile group reinforces the soil mass underneath the raft foundation, the lateral wall displacement will be largely reduced in deep excavation. Maximum lateral wall displacements with piled-raft foundations only approximate 25% of those with unpiled-raft foundations (or $(\delta_{h\text{-}max})_{3D}^{piled} \approx 0.25 \times (\delta_{h\text{-}max})_{3D}^{unpiled}$). As a consequence, neglecting the pile foundation in numerical model may decrease the retaining capacity of diaphragm wall and over-predict the lateral wall displacement. In addition, the maximum lateral wall displacement occurs just below the excavation bottom for piled-raft cases whereas it locates at a deeper position below the excavation bottom for unpiled-raft cases. Moreover, the *PSR* of unpiled-raft cases is constantly smaller than that of piled-raft cases and this indicates that the corner effect in deep excavation with the unpiled-raft is more noticeable than that with the piled-raft. It can also be deduced that for the plain strain condition the maximum lateral displacement with the unpiled-raft is larger than 4 times of that the piled-raft (or $(\delta_{h\text{-}max})_{2D}^{unpiled} > 4.0 \times (\delta_{h\text{-}max})_{2D}^{piled}$).

In deep excavation phase, other than the magnitude of ground settlement, the settlement pattern of the ground surface outside the excavation area with the piled-raft is different from that with the unpiled-raft. The piled-raft case shows a ground settlement of spandrel type pattern while the unpiled-raft case exhibits a ground settlement of concave type pattern.

Under the structure loading, the raft bending moment pattern is similar to the raft settlement pattern. For the unpiled-raft, the raft appears a concave settlement pattern at the central area which alternately causes a larger bending moment. However, the piled-raft has a uniform settlement pattern which is consequently associated with a smaller bending moment.

In summary, a raft with pile group not only enables to promote the retaining capacity of diaphragm wall but also to mitigate the differential settlement and bending moment of a raft foundation. Therefore, it is crucial and recommended to have a more realistic numerical modeling on a piled-raft foundation in deep excavation by including the pile group in the numerical model.

REFERENCES

Bourgeois, E., De Buhan, P. and G. Hassen (2012). Settlement analysis of piled-raft foundations by means of a multiphase model accounting for

soil-pile interactions. Computers and Geotechnics 46, 26-38.

Chen, S. Y. (2014). Three-dimensional analysis of piled-raft foundation in deep excavation of Taipei metropolitan, Master Thesis, National Chung Hsing University, Taichung, Taiwan.

Chen, Z. M. (2002). Three dimensional numerical analysis of piled raft foundations in Taipei metropolitan, Master Thesis, National Cheng Kung University, Tainan, Taiwan.

Chou, J. C. (2002). Numerical analysis of corner effect and creep behavior for deep excavation of high-rise building in Taipei Metropolitan, Master Thesis, National Cheng Kung University, Tainan, Taiwan.

Comodromos, E. M., M. C. Papadopoulou and I. K. Rentzeperis (2009). Pile foundation analysis and design using experimental data and 3-D numerical analysis. Computers and Geotechnics 36(5), 819-836.

Hsieh, P. G. and C. Y. Ou (1998). Shape of ground surface settlement profiles caused by excavation. Canadian geotechnical journal 35(6), 1004-1017.

Karim, H. H., M. R. AL-Qaissy and M. K. Hameedi (2013). Numerical Analysis of Piled Raft Foundation on Clayey Soil. Eng. & Tech. Journal 31, Part (A), No.7, 1297-1312

Lee, S. W., W. W. L. Cheang, W. M. Swolfs and R. B. J. Brinkgreve (2010). Modelling of piled rafts with different pile models. In Proceedings of the 7th European Conference on Numerical Methods in Geotechnical Engineering. Trondheim, Norway: CRC Press (637-642).

Liang, F. Y., L. Z. Chen and X. G. Shi (2003). Numerical analysis of composite piled raft with cushion subjected to vertical load. Computers and Geotechnics 30(6), 443-453.

Lin, D. G. and S. M. Woo (2000). Deformation analysis of Taipei International Financial Center deep excavation project, technical report. Trinity Foundation Engineering Consultants Co., LTD.

Lin, D. G. and S. M. Woo (2005). Geotechnical analyses of Taipei International Financial Center (Taipei 101) Construction Project, 16th International Conference on Soil Mechanics and Geotechnical Engineering, 1513-1516, September 12-16, 2005, Osaka, Japan

Long, P. D. (2010). Piled raft-a cost-effective foundation method for high-rises. Geotechnical Engineering 41(3), 1-12.

Nguyen, D. D. C., S. B. Jo and D. S. Kim (2013). Design method of piled-raft foundations under vertical load considering interaction effects. Computers and Geotechnics 47, 16-27.

Nguyen, D. D. C., D. S. Kim and S. B. Jo (2014). Parametric study for optimal design of large piled raft foundations on sand. Computers and Geotechnics 55, 14-26.

Oh, E. Y. N., Q. M. Bui, C. Surarak and A. S. Balasurbamaniam (2009). Investigation of the Behavior of Piled Raft Foundations in Sand by Numerical Modeling. In The Nineteenth International Offshore and Polar Engineering Conference. International Society of Offshore and Polar Engineers.

Poulos, H. G., J. C. Small and H. Chow (2011). Piled raft foundations for tall buildings. Geotechnical Engineering Journal of the SEAGS and AGSSEA 42(2), 78-84.